Microfluid Nanofluid (2014) 17:1053–1060
DOI 10.1007/s10404-014-1391-1

RESEARCH PAPER

Strong mechanical coupling between the carbon nanotube and the inner streaming water flow

Y. D. Kuang · S. Q. Shi

Received: 24 September 2013 / Accepted: 23 March 2014 / Published online: 31 March 2014

Abstract The mechanical coupling between the carbon nanotube (CNT) and the inner streaming water flow is investigated using non-equilibrium molecular dynamics simulations. A strong coupling is found at a critical streaming velocity and such coupling results in the local buckling of single-walled or multi-walled CNTs. The flow-excited radial resonance and the drastic energy exchange-induced radial deformation amplification of the tube contribute to the occurrence of buckling. The tube instability in turn gives rise to the unstable water transport. In contrast to instability occurrence of lamped–lamped macropipes conveying fluid, fully fixing tube's boundary atoms may eliminate such instability. Combined with the finite element analysis, the effects of the tube size, hydrostatic pressure, van der Waals interaction strength, and the tube wall number on the buckling are discussed. The unusual result is that increasing the hydrostatic pressure weakens the tube's stability.

Keywords Carbon nanotubes · Molecular flow · Buckling instability · Non-equilibrium molecular dynamics simulations · Finite element analysis

1 Introduction

Carbon nanotubes (CNTs) (Qin et al. 2000) possess many exceptional mechanical properties, such as high elastic modulus, large elastic strain, and strong breaking strain sustaining capability. Moreover, they have a hollow cylindrical geometry and stable structures formed by sp^2 carbon atoms. Therefore, CNTs are believed to make ideal nanopipes for transport of nanofluidic or biological molecules or for water purification and desalination (Falk et al. 2010; Walther et al. 2013; Humplik et al. 2011). CNT-based nanofluidic devices such as nanovalves (Maniwa et al. 2007), nanofluidic sensors (Ghosh et al. 2003), and nanopumps (Insepov et al. 2006; Duan and Wang 2010) have already been reported in the literature and have shown promising applications.

The ultra-fast transport of water in CNTs had been observed in both experiments (Sholl and Johnson 2006; Majumder et al. 2005) and molecular dynamics (MD) simulations (Joseph and Aluru 2008), and the flow rate was thought to be much higher than would be predicted by classical continuum fluid mechanics. It was suggested (Joseph and Aluru 2008; Huang et al. 2008) that the water in inside a CNT has a non-wetting behavior and that a depletion area between the carbon wall and the first water layer is responsible for the ultra-low friction and the ultra-fast flow, while Walther et al. (2013) argued that anomalously high flow rate enhancement ratio reported in previous experimental and MD studies cannot be attributed solely to interactions of water with pristine CNTs based on their MD simulation results, in which a good agrement between their MD results and those by the previous experiment (Qin et al. 2011) was obtained. Related to such a binary system, previous studies mainly focused on three aspects. The first is related to fluidic properties (Nanok et al. 2009), including quasi-static properties such as diffusion (Striolo 2006) or confinement-induced phase transformation (Koga et al. 2001) and transport dynamics (Insepov et al. 2006; Nanok et al. 2009; Hummer et al. 2001). The second is related to the wall/water interface in

Y. D. Kuang · S. Q. Shi (✉)
Department of Mechanical Engineering,
Hong Kong Polytechnic University,
Hung Hom, Kowloon, Hong Kong
e-mail: mmsqshi@polyu.edu.hk

regard to the wetting and slip properties of the carbon wall (Walther et al. 2013). The third is related to the properties of CNTs, including the environment-dependent phonon mode (Longhurst and Quirke 2007) and electron movement in CNTs by direct water drag (Ghosh et al. 2003).

When investigating the quasi-static properties of the inner fluid, treating CNTs as rigid body was thought a proper approximation under equilibrium conditions, and such treatment was applied in some equilibrium MD (EMD) simulations (Sholl and Johnson 2006; Nanok et al. 2009; Longhurst and Quirke 2007). Meanwhile, to focus on the fluid flow behaviors in CNTs or the interfacial slip behavior, most non-equilibrium MD (NEMD) simulations also treated the CNTs as rigid bodies (Chen et al. 2008) and neglected the thermal movement of the carbon atoms for simplicity. However, the application of such treatment to CNTs with inner fluid requires special caution. Chen et al. (2006) reported that the inclusion of nanotube flexibility in EMD simulations reduces the gas diffusivity by roughly an order of magnitude. This result shows that CNT dynamics affect the fluid behaviors to a noticeable degree. Chen et al. (2011) found that significant energy exchange occurs between the thermal CNT and surrounding water flow in their NEMD simulations. Furthermore, Longhurst and Quirke (2007) observed the upshift of the radial breathing mode frequency of the CNT due to the van der Waals (vdWs) interaction with the surrounding water in their EMD simulations. These results reveal that the vdWs interaction between the tube wall and the water molecules changes the dynamics of the CNT itself, whether for quasi-static water (Longhurst and Quirke 2007) or for streaming water (Chen et al. 2008). In contrast to the focus on flow behaviors or slip properties in thermal or rigid CNTs or the focus on the effect of surrounding water on CNT dynamics in the previous literature, the interplay between the thermal CNT and the inner fluid flow by radial vibration modes has not been understood thoroughly. Clearly understanding such interplay will provide insights into not only CNT dynamics but also nanofluidic behaviors.

In this work, one type of interplay effect, i.e., the mechanical dynamic coupling between the CNT's radial vibration mode and the inner water flow is observed in our NEMD simulations. Interplay-induced buckling instability for single-walled, double-walled, and multi-walled CNTs is found. This tube instability in turn results in unstable transport of the inner water. Following this observation and the corresponding discussion on the mechanism for such buckling, the effects of tube size, tube/water vdWs interaction strength, hydrostatic pressure, and tube wall number on the buckling are further explored using NEMD simulations and finite element (FE) simulations.

2 Simulation methods

2.1 Non-equilibrium molecular dynamics simulations

In our NEMD simulations based on the open-source code LAMMPS (Plimpton 1995), the second-generation Brenner potential (Brenner et al. 2002) and TIP3P water model are used for the atomistic interaction in single-walled CNTs (SWCNTs) and in water molecules, respectively. The electrostatic interaction between water molecules is calculated using the PPPM arithmetic. The Lennard–Jones parameters (Hummer et al. 2001) relative to C and O atoms are $\sigma_{C-C} = 0.3400$ nm, $\varepsilon_{C-C} = 0.0037$ eV, $\sigma_{C-O} = 0.3188$ nm, and $\varepsilon_{O-O} = 0.0044$ eV. The cutoff for the electrostatic interaction and vdWs interaction is taken as 1 nm. The number of water molecules in each SWCNT is given based on the density 0.98 g/cm^3. Only the periodic boundary condition of the axial direction is kept for such CNT/water binary systems, which are relaxed at a temperature of 300 K with the hydrostatic pressure at 1.0 atm for the inner water. Then, the water flow is established by a gravity-driven approach[15] along the axial direction. After the expected streaming velocity is obtained, the gravity-like acceleration is removed, and the water molecules will move without constraint except for collisions with the tube wall. During the acceleration and no acceleration conditions, the temperature of the SWCNT is controlled at 300 K by a Noose–Hoover thermostat. The axial degree of freedom of one end carbon atom is constrained to prevent axial movement of the mass center of the tube. A series of parallel simulations with time step of 1 fs are conducted for such systems with different sizes. The diameter and the length of SWCNTs range from 2.71 to 6.78 nm and from 7.38 to 68.87 nm, respectively. The corresponding number of water molecules and carbon atoms ranges from 890 to 8260 and from 2,400 to 22,400, respectively.

2.2 Finite element simulations

In our FE calculations based on the code ANSYS 14.0, in order to get the mode frequency and the mode shape of a CNT at continuum level, the CNT is regarded as a thin isotropic shell and then the standard vibrational mode analysis in this code is conducted to solve the eigenvalue problem under given mechanical loading and boundary conditions. The mode shape represents the relative vibration amplitude at given mode frequency. The hydrostatic pressure is applied by imposing the loading along the radial direction of the shell. The axial displacement constraint corresponding to that in our MD simulations is taken as the mechanical boundary condition in the FE calculations. As the basic input, the element type is given as SHELL181 with a thickness of 0.34 nm, and the density and the

Poisson ratio are taken as 2.27 g/cm^3 and 0.16, respectively (Longhurst and Quirke 2007). Considering the diameter-dependent in-plane rigidity previously reported by Xiao and Liao (Xiao and Liao 2002) and the proportional relation between the in-plane rigidity and the elastic modulus, the elastic modulus is taken proportionally from 1.16 to 1.06 TPa as the SWCNT diameter increases from 2.7 to 4.5 nm. For SWCNTs larger than 4.5 nm, the elastic modulus remains at 1.06 TPa.

3 Phenomenon of buckling instability and its mechanism

Figure 1 shows the velocity evolution over time as an initial flow velocity of 3,000 m/s is established in the (20, 20) SWCNT having a length of 14.78 nm. The potential energy evolution for this SWCNT is also shown in this figure. The SWCNT loses its stability in the form of local buckling (Yakobson et al. 1996) at a critical flow velocity of 2,630 m/s, and the corresponding potential energy of the tube decreases to a lowest value of −37,285 eV. From the NEMD simulation trajectories, we observed that before buckling, the radial resonance of the tube wall is excited by the water flow after about 10 ps. The radial resonance mode has a circumferential half-wave number of $m = 2$ (See the second tube in the inset). For the SWCNT itself, this radial resonance increases the radial deformation and the potential energy of the tube compared with its stable equilibrium state. However, the resonance causes the inner water to suffer from a periodical beat by the tube wall. In turn, the beat patter-induced abrupt reduction in the tube cross-section makes the kinetic energy of the water flow transfer into the tube and further increases the potential energy and radial displacement of the tube. Consequently, the resonance mode possesses larger radial vibration amplitude and smaller cross-section, which again result in more kinetic energy of the water flow being transferred into the tube and further increase its potential energy and deformation until the excessive radial deformation causes the tube wall to buckle locally. As observed in our NEMD simulations, the drastic energy exchange between the tube and the water flow causes the radial deformation to increase gradually up to 2 angstroms at 25 ps. After 25 ps, the tube wall can no longer sustain the elastic deformation of the resonance mode and evolves into the buckling phase. As expected, the buckling mode has the same shape (third tube in the inset) as that of the resonance mode. Therefore, the flow-induced resonance of the tube wall and the continuous energy exchange-induced deformation amplification mechanism contribute to the buckling instability. We also conducted NEMD simulations without temperature control and by controlling the tube temperature to lower

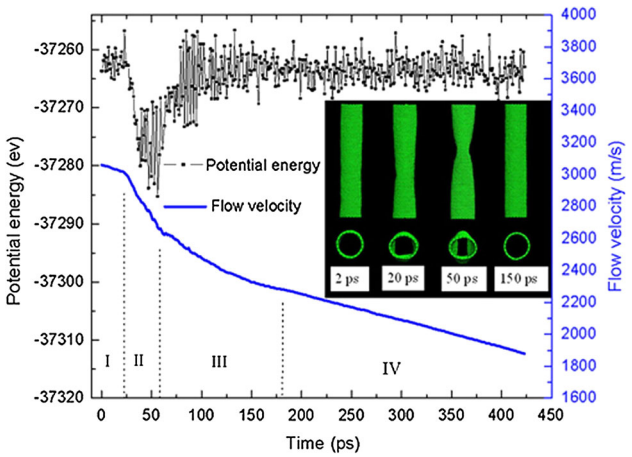

Fig. 1 The flow velocity drop and the potential energy variation of the (20, 20) SWCNT with four phases from *I* to *IV*. (*I*) Accumulation phase during 0–25 ps: the velocity descends linearly, and the potential energy and the radial deformation of the SWCNT increase gradually. In the *inset*, the time indices of 2 and 20 ps correspond to the original state and the elastic resonance state, respectively. The water molecules are not shown for clarity. (*II*) Buckling phase during 25–55 ps: the velocity descends drastically and buckling of the SWCNT occurs and continues. In the *inset*, the time index 50 ps corresponds to the buckling state; (*III*) Buckling degradation phase during 55–178 ps: the velocity descends non-linearly, and the potential energy gradually increases accompanied by a decrease in the buckling deformation. In the *inset*, the time index 150 ps corresponds to the buckling degradation state. (*IV*) Stable phase from 178 ps to the end: the velocity will descend linearly to zero at last due to collisions with the tube wall, and the potential energy fluctuates slightly around a constant value

than 300 K, both of which give the critical flow velocity of 2,630 m/s, showing that buckling is an intrinsic behavior of this binary system. For the (30, 8) SWCNT and the (35, 0) SWCNT having the same diameter and length with those of the (20, 20) SWCNT, NEMD simulations show that the chirality has little effect on the critical flow velocity and buckling mode.

The present buckling mechanism involves a dynamic process that is greatly different from previously reported buckling caused by external quasi-static loading such as axial pressure (Yakobson et al. 1996) and bending loading (Wang et al. 2006). The mechanism of quasi-static buckling of CNTs is that the tube wall releases some strain energies to reach a metastable state, i.e., the buckling state when the excessive axial pressure or strain is applied. The present buckling is involved with this just-mentioned mechanism rather than external axial pressure or strain, this point can be further proved by the axial force fluctuation extracted from our NEMD simulations just before the buckling of this (20, 20) SWCNT. This is plotted in Fig. 2a, where the plus and the minus values in this figure denote the axial tensile and compressive forces, respectively. The compressive force is caused mainly by the

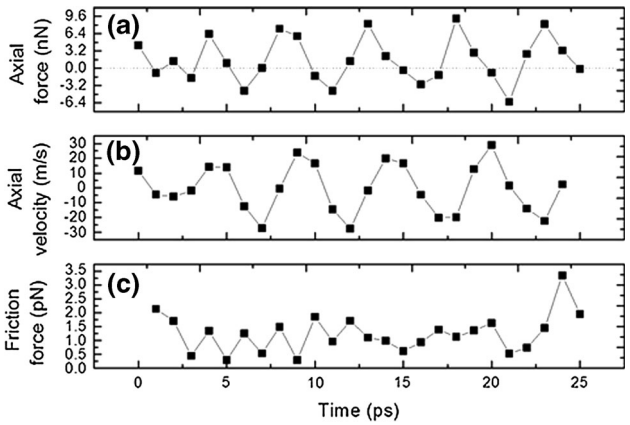

Fig. 2 The axial force fluctuation (**a**), the axial velocity fluctuation (**b**), and the friction force (**c**) before buckling

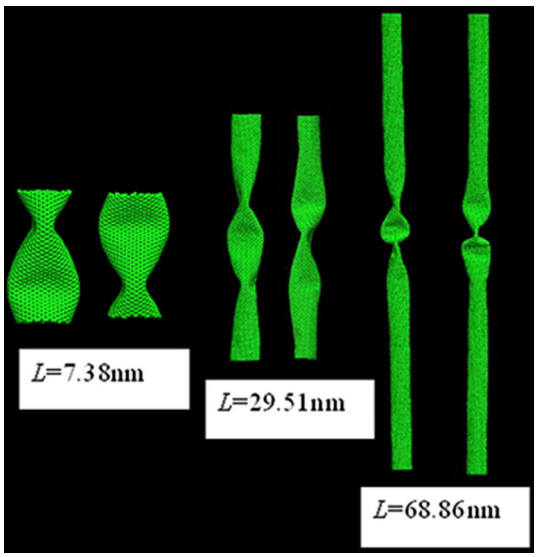

Fig. 3 Buckling topologies of the pure (20, 20) SWCNTs with different lengths; each has two visual angles with 90° intersections

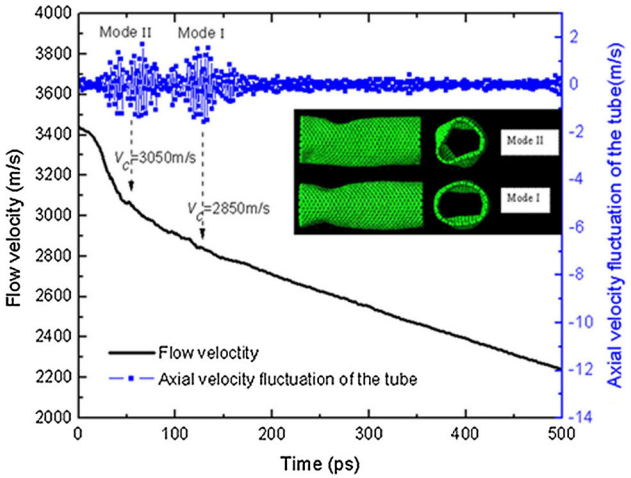

Fig. 4 Buckling mode transition in a (20, 20) SWCNT having a length of 7.38 nm

radial vibration of the SWCNT itself, which results in the axial velocity fluctuation of this SWCNT, as seen in Fig. 2b. In contrast, the compressive force is two orders of magnitude lower than the critical buckling pressure of this pure SWCNT, which is about 113 nN as extracted from our NEMD simulations (see the following discussion). Therefore, the fluctuating axial pressure is not the main reason for the buckling. The maximum tensile amplitude in Fig. 2a is obviously higher than that of the compression amplitude, implying the SWCNT experiences a net tensile force up to nN order amplitude after subtracting the vibration-induced axial compressive force. Considering the vdWs repulsive effect and the almost incompressible inner water, it is reasonably expected that the inward radial resonance displacement is slightly smaller than the outward displacement during the energy exchange process. Therefore, with the constraint at the tube end, there must be a net tensile force according to the force equilibrium. Moreover, the water drag-induced interfacial friction f also contributes to the net tensile force, f is given as $f = m\Delta U/\Delta t$, in which m is the collective water mass and ΔU is the water velocity increment during the period Δt. It can be seen that the friction shown in Fig. 2c has only pN order of amplitude, showing the super smoothness of the wall as observed in previous experiments (Sholl and Johnson 2006; Majumder et al. 2005) and MD simulations (Joseph and Aluru 2008).

For those (20, 20) SWCNTs conveying water, their buckling topologies have only one symmetric collapse zone for all considered lengths except for the length 68.87 nm (see Figs. 1, 4 and 5a). However, for the corresponding pure SWCNTs under axial pressure, our NEMD simulations with a reasonable strain ratio 1.3×10^9 per second show that their buckling topologies have two collapse zones along the axial direction as seen in Fig. 3. The filling effect of the inner water may contribute to the fewer collapse zones in the SWCNT conveying water.

Interestingly, we also observe a buckling mode transition (Fig. 4) from $m = 3$ (Mode II) to $m = 2$ (Mode I) for the given (20, 20) SWCNT with a length of 7.38 nm if an initial flow velocity of 3,430 m/s is established. The resonance mode with $m = 3$ is activated at first and then evolves into the high-order buckling mode with $m = 3$. The calculated axial velocity fluctuation of the tube shows two peaks: one corresponds to the high-order buckling mode at a critical flow velocity of 3,050 m/s, and the other corresponds to the low-order buckling mode ($m = 2$) at a critical flow velocity of 2,850 m/s. The buckling-induced drastic radial breathing deformation contributes to the

significant fluctuation in axial velocity. Similar to this (20, 20) SWCNT, the other SWCNTs also possess this behavior of the mode transition. In the following discussion, the critical flow velocity refers to the lowest velocity if not otherwise specified.

4 Effects of tube size, interfacial vdWs interaction strength, hydrostatic pressure, and wall number

We further explore the effects of the length (Fig. 5a) and diameter (Fig. 5b) of SWCNTs on the buckling. It can be seen that those SWCNTs with different length have the same buckling topological structures with mode number $m = 2$. Although those SWCNTs with different diameters develop buckling structures with mode numbers from

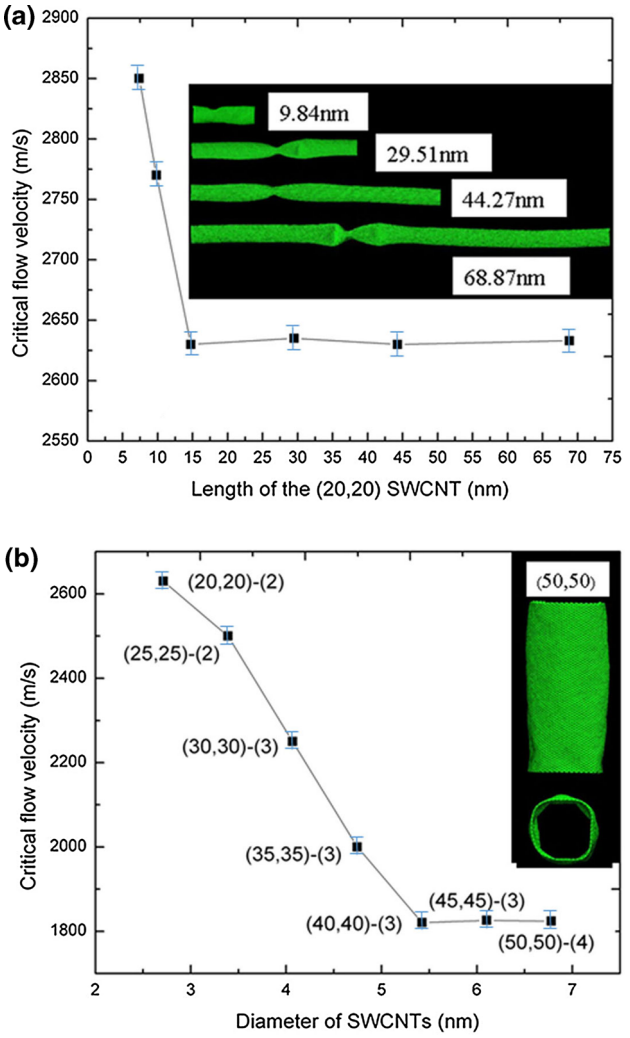

Fig. 5 The effects of length (**a**) and diameter (**b**) of the (20, 20) SWCNT on the critical velocity. In the index (i, j)-(m), (i, j), and (m) denote the SWCNT chirality and the circumferential half-wave number of the buckling mode, respectively

$m = 2$ to $m = 4$, the general trend is that larger tubes have a higher buckling mode order. Moreover, Fig. 5a and b show a similar trend: there is little decrease in critical velocity after the length or the diameter reaches a certain threshold value.

The cost to calculate such size effects, as shown in Fig. 5 using parallel simulations, is expensive. Thus, the question naturally rises: can the classical theory of fluid–solid coupling dynamics, i.e., the shell theory combined with the linear potential fluid theory (Paidoussis and Denise 1972), predict such trends? If so, the cost of calculations may be efficiently saved. At the macroscale, previous theoretical and experimental work (Paidoussis and Denise 1972) on thin shells conveying fluid found that shells may buckle under the clamped–clamped mechanical boundary condition. Is the same true for nanoscale shells conveying fluid? Previous MD simulations (Yakobson et al. 1996) validated the feasibility of applying the shell theory to predict buckling properties and the pressure dependence of the radial breathing mode (Longhurst and Quirke 2007) of pure SWCNTs, and buckling under such mechanical boundary conditions was also observed for given pressure loading. Moreover, recent work (Thomas and McGaughey 2009) has shown that a continuum description of water flow is appropriate for CNTs with diameter greater than 1.6 nm. However, after fully fixing all of the end carbon atoms, our MD simulations showed that the (20, 20) SWCNT with a length of 14.78 nm does not lose its stability even if high enough flow velocity is established. This result does not match with that corresponding to the macrosize shells or pure SWCNTs with the same mechanical boundary conditions. The reasons for the good stability are that fully fixing all of the end carbon atoms constrains the development of the radial resonance mode, and the deformation amplification mechanism cannot work. In contrast to the direct application of the classical theory of fluid–shell coupling dynamics to analyze the instability of such nanoscale systems in the previous literature (Yan et al. 2007), the present simulation shows that the corresponding classical theory fails to predict the local buckling. It is also noticed in literature that Hagen–Poiseuille equation is modified to describe the flow rate enhancement ratio in CNTs. There is a large scatter of the enhancement ratio ranging from 10 to 10^5 in the reported experiments or simulations, even including some contradictory results on the dependence on the CNT diameter (Thomas et al. 2010). While the length-dependent enhancement was well elucidated by Walther et al. (2013), further study is still needed to further our understanding on such topic.

Noticing the vibration mode-dependent critical flow velocity, we attempt to evaluate the size-dependent mode frequency so as to qualitatively characterize the trends

observed in Fig. 5. Although the analytical shell model (Longhurst and Quirke 2007) for the radial breathing mode frequency gave results comparable with those by EMD simulations, the shell model cannot be used here because all of the present modes are non-axisymmetric and have higher order. Therefore, the FE method is used to calculate the mode frequencies. The frequency results corresponding to the mode order and tube size in Fig. 5 are shown in Fig. 6a, b. It can be seen that effects of length and diameter on the mode frequency show the same trends as those in Fig. 5a, b. Representatively, the resonance-mode shapes for (20, 20), (35, 35), and (50, 50) SWCNTS having the same length of 14.78 nm are shown in Fig. 6d. They present similar topologies with those observed in our NEMD simulations. The present comparisons justify that the mode frequency is the direct index of the critical flow velocity. The effect of the hydrostatic pressure is also shown in Fig. 6c, which will be discussed below.

It is well known that the SWCNT and water interplay by the vdWs interface. Therefore, the effect of the wall/water interaction strength on buckling is investigated for the SWCNT with a length of 14.78 nm. As shown in Fig. 7a, increasing the vdWs interaction greatly by 30 % results in reducing the critical velocity by 6 % and vice versa. Further analysis shows that frictional force f is increased by about 20 %, implying that the increase in vdWs interaction well results in the larger interfacial pressure (Barrat 1999). To directly elucidate the effect of the interfacial pressure on the dynamical stability of the tube, the hydrostatic pressures of 0.2 and 0.4 GPa, i.e., the interfacial pressures, are produced after applying axial strains of 0.002 and 0.004, respectively, to the whole system. It should be noted that the axial strains have little effect on the static mechanical stability of the SWCNT itself because they are one order lower than the corresponding static buckling strain of 0.04. Meanwhile, the hydrostatic pressure of the water filling has a positive effect on the static mechanical stability of the SWCNT (Ni et al. 2002). In contrast to that for static stability, the hydrostatic pressure decreases the dynamical stability, i.e., the critical velocity as shown in Fig. 7b, which also proves the results in Fig. 7a. From the viewpoint of mode frequency, the FE result shown in Fig. 6c reveals that increasing the hydrostatic pressure results in a lower resonance-mode frequency. Consequently, considering the direct correlation between the mode frequency and the critical flow velocity, it can be concluded that the critical velocity also decreases, which matches with the results in Fig. 7b.

The effect of tube wall number is also investigated. For the SWCNT just mentioned, increasing the tube wall

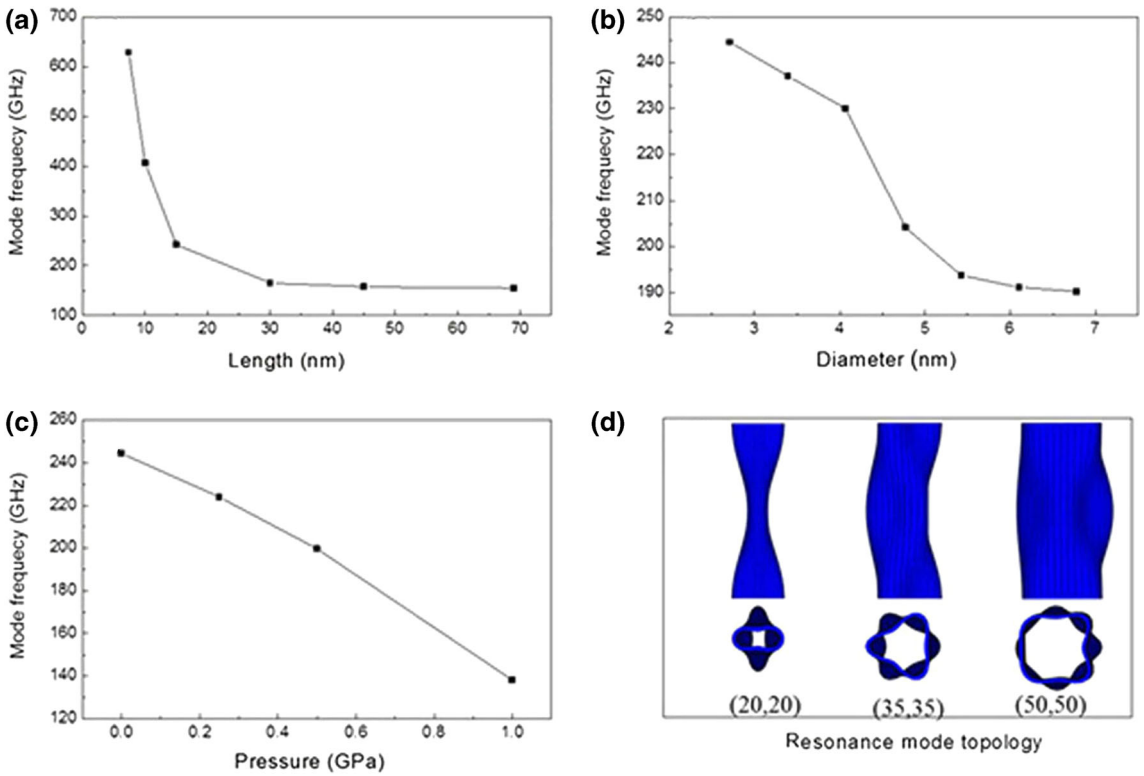

Fig. 6 Effects of length (**a**), diameter (**b**) and hydrostatic pressure (**c**) on the resonance-mode frequencies of SWCNTs by the FE method together with the mode shapes (**d**)

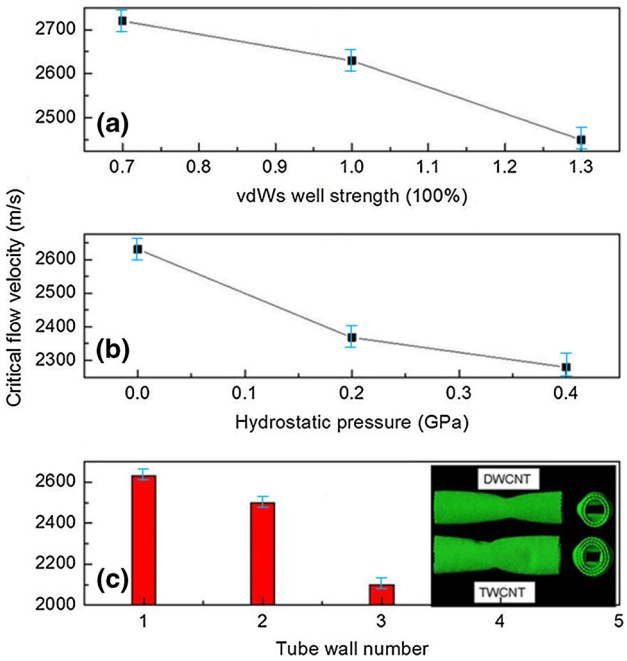

Fig. 7 Effects of (**a**) the carbon/water interaction strength, (**b**) hydrostatic pressure, and (**c**) tube wall number on the critical flow velocity

number to 2 and 3 gradually reduces the critical velocity (see Fig. 7c), and the corresponding double-walled (DW) and triple-walled (TW) CNTs, i.e., (20, 20)@(25, 25) DWCNT and ((20, 20)@(25, 25))@(30, 30) TWCNT have the same buckling mode order number $m = 2$ as that of the (20, 20) SWCNT. However, in a sense of continuum, it seems that increasing the wall number is equivalent to increasing the wall thickness and thus enhancing the wall stability. Two reasons explain this interesting result. One is that each layer in the DWCNT or the TWCNT buckles collaboratively by the intertube vdWs interaction and has the same buckling mode. The other is that the DWCNT or the TWCNT has weaker mechanical stability than the innermost tube (Kuang et al. 2010), and the critical flow velocity mainly depends on the outermost tube. A proof for this can be found from Figs. 5b and 7c in which the (25, 25) SWCNT has the same critical flow velocity of 2,500 m/s as that of the (20, 20)@(25, 25) DWCNT. Moreover, the (30, 30) SWCNT has a higher critical flow velocity than the ((20, 20)@(25, 25))@(30, 30) TWCNT because this SWCNT has a higher-order buckling mode number $m = 3$. In contrast to the outermost tube dominant critical velocity, the same buckling mode among the SWCNT, the DWCNT and the TWCNT show that the innermost tube determines the buckling mode. Further, considering the obtained result together with the results in Figs. 5b and 6b, it can be reasonably expected that the critical velocity for MWCNTs will decrease slightly as the given outermost tube diameter increases beyond about 5 nm.

5 Concluding remarks

NEMD simulations are conducted to investigate the interplay dynamics between SWCNTs and inner water flow. It is observed that the tube wall buckles locally at a critical flow velocity. The radial resonance activated by the flow and the radial deformation amplification due to energy exchange contribute to the buckling instability. In turn, the buckling-induced large deformation of the tube results in the unstable flow of the inner water. The tube chirality has no effect on the critical velocity. The good stability for clamped–clamped SWCNTs due to the constraint of the radial deformation amplification process shows the unsuitableness of the classical theory of fluid–shell coupling dynamics for such binary systems.

Combined with FE analysis, NEMD simulation results show that the critical velocity changes little after the length or the diameter of the tube reaches a certain threshold value. The increase in the tube/water vdWs interaction strength, the hydrostatic pressure, or the tube wall number may reduce the critical velocity. The comparison between FE results and those from NEMD simulations justifies the finding that tube mode frequency is a direct index of the critical velocity. The present work also provides direct insights for the interplay dynamics of other types of nanotubes or nanofluids.

Acknowledgments This work is supported by grants from the Research Grants Council of Hong Kong (B-Q19A and E-RD39).

References

Barrat J-L (1999) Influence of wetting properties on hydrodynamic boundary conditions at a fluid/solid interface. Faraday Discuss 112:119–128

Brenner DW, Shenderova OA, Harrison JA, Stuart SJ, Ni B, Sinnott SB (2002) A second-generation reactive empirical bond order (REBO) potential energy expression for hydrocarbons. J Phys-Condens Matter 14(4):783–802. doi:10.1088/0953-8984/14/4/312

Chen HB, Johnson JK, Sholl DS (2006) Transport diffusion of gases is rapid in flexible carbon nanotubes. J Phys Chem B 110(5):1971–1975. doi:10.1021/Jp056911i

Chen X, Cao GX, Han AJ, Punyamurtula VK, Liu L, Culligan PJ, Kim T, Qiao Y (2008) Nanoscale fluid transport: size and rate effects. Nano Lett 8(9):2988–2992. doi:10.1021/Nl802046b

Chen C, Ma M, Jin K, Liu JZ, Shen LM, Zheng QS, Xu ZP (2011) Nanoscale fluid-structure interaction: flow resistance and energy transfer between water and carbon nanotubes. Phys Rev E 84(4):046314. doi:10.1103/Physreve.84.046314

Duan WH, Wang Q (2010) Water transport with a carbon nanotube pump. ACS Nano 4(4):2338–2344. doi:10.1021/Nn1001694

Falk K, Sedlmeier F, Joly L, Netz RR, Bocquet L (2010) Molecular origin of fast water transport in carbon nanotube membranes: superlubricity versus curvature dependent friction. Nano Lett 10(10):4067–4073. doi:10.1021/Nl1021046

Ghosh S, Sood AK, Kumar N (2003) Carbon nanotube flow sensors. Science 299(5609):1042–1044. doi:10.1126/science.1079080

Huang DM, Sendner C, Horinek D, Netz RR, Bocquet L (2008) Water slippage versus Contact angle: a quasiuniversal relationship. Phys Rev Lett 101(22):226101. doi:10.1103/Physrevlett.101.226101

Hummer G, Rasaiah JC, Noworyta JP (2001) Water conduction through the hydrophobic channel of a carbon nanotube. Nature 414(6860):188–190. doi:10.1038/35102535

Humplik T, Lee J, O'Hern SC, Fellman BA, Baig MA, Hassan SF, Atieh MA, Rahman F, Laoui T, Karnik R, Wang EN (2011) Nanostructured materials for water desalination. Nanotechnology 22(29):292001. doi:10.1088/0957-4484/22/29/292001

Insepov Z, Wolf D, Hassanein A (2006) Nanopumping using carbon nanotubes. Nano Lett 6(9):1893–1895. doi:10.1021/Nl060932m

Joseph S, Aluru NR (2008) Why are carbon nanotubes fast transporters of water? Nano Lett 8(2):452–458. doi:10.1021/Nl072385q

Koga K, Gao GT, Tanaka H, Zeng XC (2001) Formation of ordered ice nanotubes inside carbon nanotubes. Nature 412(6849):802–805. doi:10.1038/35090532

Kuang Y, Shi S, Chan P, Chen C (2010) The effect of intertube van der Waals interaction on the stability of pristine and functionalized carbon nanotubes under compression. Nanotechnology 21(12):125704

Longhurst MJ, Quirke N (2007) Pressure dependence of the radial breathing mode of carbon nanotubes: the effect of fluid adsorption. Phys Rev Lett 98(14):145503. doi:10.1103/Physrevlett.98.145503

Majumder M, Chopra N, Andrews R, Hinds BJ (2005) Nanoscale hydrodynamics—enhanced flow in carbon nanotubes. Nature 438(7064):44. doi:10.1038/43844a

Maniwa Y, Matsuda K, Kyakuno H, Ogasawara S, Hibi T, Kadowaki H, Suzuki S, Achiba Y, Kataura H (2007) Water-filled single-wall carbon nanotubes as molecular nanovalves. Nat Mater 6(2):135–141. doi:10.1038/Nmat1823

Nanok T, Artrith N, Pantu P, Bopp PA, Limtrakul J (2009) Structure and dynamics of water confined in single-wall nanotubes. J Phys Chem A 113(10):2103–2108. doi:10.1021/Jp8088676

Ni B, Sinnott SB, Mikulski PT, Harrison JA (2002) Compression of carbon nanotubes filled with C 60, CH 4, or Ne: predictions from molecular dynamics simulations. Phys Rev Lett 88(20):205505

Paidoussis M, Denise J-P (1972) Flutter of thin cylindrical shells conveying fluid. J Sound Vib 20(1):9–26

Plimpton S (1995) Fast parallel algorithms for short-range molecular-dynamics. J Comput Phys 117(1):1–19. doi:10.1006/jcph.1995.1039

Qin LC, Zhao XL, Hirahara K, Miyamoto Y, Ando Y, Iijima S (2000) Materials science—the smallest carbon nanotube. Nature 408(6808):50. doi:10.1038/35040699

Qin X, Yuan Q, Zhao Y, Xie S, Liu Z (2011) Measurement of the rate of water translocation through carbon nanotubes. Nano Lett 11(5):2173–2177

Sholl DS, Johnson JK (2006) Making high-flux membranes with carbon nanotubes. Science 312(5776):1003–1004. doi:10.1126/science.1127261

Striolo A (2006) The mechanism of water diffusion in narrow carbon nanotubes. Nano Lett 6(4):633–639. doi:10.1021/Nl052254u

Thomas JA, McGaughey AJ (2009) Water flow in carbon nanotubes: transition to subcontinuum transport. Phys Rev Lett 102(18):184502

Thomas JA, McGaughey AJ, Kuter-Arnebeck O (2010) Pressure-driven water flow through carbon nanotubes: insights from molecular dynamics simulation. Int J Therm Sci 49(2):281–289

Walther JH, Ritos K, Cruz-Chu ER, Megaridis CM, Koumoutsakos P (2013) Barriers to superfast water transport in carbon nanotube membranes. Nano Lett 13(5):1910–1914. doi:10.1021/Nl304000k

Wang JB, Guo X, Zhang HW, Wang L, Liao JB (2006) Energy and mechanical properties of single-walled carbon nanotubes predicted using the higher order Cauchy-Born rule. Phys Rev B 73(11):115428. doi:10.1103/Physrevb.73.115428

Xiao T, Liao K (2002) Nonlinear elastic properties of carbon nanotubes subjected to large axial deformations. Phys Rev B 66(15):153407. doi:10.1103/Physrevb.66.153407

Yakobson BI, Brabec CJ, Bernholc J (1996) Nanomechanics of carbon tubes: instabilities beyond linear response. Phys Rev Lett 76(14):2511–2514. doi:10.1103/PhysRevLett.76.2511

Yan Y, He X, Zhang L, Wang Q (2007) Flow-induced instability of double-walled carbon nanotubes based on an elastic shell model. J Appl Phys 102(4):044307